Channel structures in alkali-metal-doped conjugated polymers: Broken-symmetry two-dimensional intercalation superlattices

P. A. Heiney,* J. E. Fischer,† D. Djurado,‡ and J. Ma*
Laboratory for Research on the Structure of Matter, University of Pennsylvania, Philadelphia, Pennsylvania 19104

D. Chen and M. J. Winokur
Department of Physics, University of Wisconsin, Madison, Wisconsin 53706

N. Coustel§ and P. Bernier
Groupe de Dynamique des Phases Condensees, Universite Montpellier II, 34095 Montpellier CEDEX, France

F. E. Karasz
Department of Polymer Science and Engineering, University of Massachusetts, Amherst, Massachusetts 01003
(Received 18 January 1991)

Conjugated polymers doped with alkali metals typically exhibit ordered two-dimensional (2D) superlattices of linear chains and alkali-metal channels, analogous to guest-host monolayer sequences in layer intercalates. A common feature is a superlattice periodicity that varies with dopant concentration. Unique to doped polymers, the local 2D symmetry that defines the superlattice building block can vary with concentration and with the relative sizes of the dopant and chain projection normal to its axis. We present x-ray-diffraction measurements of stage-2 and stage-1 K-doped *trans*-polyacetylene, and of stage-1 Cs-doped polyparaphenylene vinylene (PPV). In all three cases, detailed profile fits are inconsistent with the highly symmetric intercalation channels previously proposed. We give evidence for new structural models in which the symmetries are broken by rotations and translations of the polymer chains. In the case of stage-2 K-$(CH)_x$, this takes place by a rotation and translation of $(CH)_x$ chains, lowering the 2D lattice symmetry from *P4mm* to *P4*. In stage-1 K-$(CH)_x$, translational distortions reduce the symmetry from *P4mm* to *P4gm*, while in stage-1 Cs-PPV a similar local symmetry reduction arises from chain rotations that do not affect the space-group symmetry. We offer several candidates as the driving force for the broken symmetries and discuss the implications for phase-diagram and band-structure calculations.

I. INTRODUCTION

It is now well established that doping of conjugated polymers with alkali metals leads to ordered dopant superlattices that may be viewed as two-dimensional analogs of the one-dimensional "stages" that occur in intercalated layer compounds. Detailed knowledge of these structures, and the interactions that stabilize them, will play a central role in elucidating the novel macroscopic properties of doped polymers. Furthermore, doped polymers constitute a second class of structures, complementary to layer intercalates, for studying the general problem of phase transitions and phase equilibria in low-dimensional guest-host systems with competing interactions.

The first diffraction evidence for ordered alkali-metal superlattices in polyacetylene, $(CH)_x$, appeared in 1983.[1] Shortly thereafter, the existence of different superlattices at varying alkali-metal concentrations was inferred from electrochemical doping experiments,[2] which showed discontinuities in open circuit voltage V_{OC} versus dopant mole fraction y. This result was suggestive of first-order phase transitions between different superlattice structures, much like the case of graphite intercalated with H_2SO_4 for which a direct correlation between electrochemical and *in situ* x-ray results had been established.[3] Discontinuities versus y were also observed from *in situ* electron spin resonance[4] and conductivity experiments.[5,6] X-ray,[7–9] neutron,[10] and electron diffraction[11] have now unambiguously confirmed the existence of ordered dopant superlattices, and in one case the correlation of $V_{OC}(y)$ discontinuities with first-order structural transitions has been established.[12]

While these data lead to a consistent picture of the gross features of alkali-metal-doped $(CH)_x$ structures, there exist several important and controversial aspects that are not well understood. One of these, the subject of this paper, is the symmetry of the guest-host building blocks, or motifs, from which the superlattices are constructed. We present detailed analyses of *in situ* and *ex situ* x-ray-diffraction data for $[(CH)K_y]_x$ which show that the high symmetries proposed in previous work, and justified in terms of simple packing and bonding arguments, are broken by previously unconsidered interactions. Similar results on Cs-doped polyparaphenylene vi-

nylene (PPV) suggest that the symmetry breaking is a general phenomenon in doped conjugated polymers.

In Sec. II we briefly review the general problem of competing interactions, contrasting the cases of layer intercalates and doped polymers. We also summarize the prevailing view of alkali-doped structures in the context of a general scheme for describing local configurations of guest and host units, or motifs, exhibiting lower symmetries than the motifs comprising the standard models. Sections III–V present x-ray data and model fits for stage-2 and stage-1 K-doped $(CH)_x$ and stage-1 Cs-doped PPV, respectively; here we show that low-symmetry motifs give much better fits to the data than high-symmetry ones. In a concluding section (Sec. VI) we suggest some possible origins for the symmetry-breaking interactions.

II. COMPETING INTERACTIONS AND LATTICE SYMMETRY

In alkali-metal-doped polymers, guest ions are arranged in "channels" parallel to the polymer chain axes. The projections of these channels onto a plane normal to the chains can be modeled as occupied sites on a two-dimensional superlattice. Thus, the two-dimensional (2D) channel projections differ in principle from a surface chemisorption system only in that the site occupancy is a continuous variable.[13] This configuration is dimensionally complementary to the layer superlattices in intercalation compounds, which consist of two-dimensional "galleries" with variable filling. In both cases the composite structure is specified by the superlattice period (or stage), the fractional occupancy of channels or galleries, and the three-dimensional correlations (if any) among guest chains and between guest and host sublattices. These structures result from the interplay among anisotropic guest-guest, guest-host, and host-host interaction energies, as well as the entropy and volume, leading to rich phase diagrams versus chemical potential μ, temperature,[13,14] and, in principle, hydrostatic pressure.

Staging superlattices are a universal feature of graphite intercalation compounds, occurring with a variety of 2D intercalate structures (disordered, commensurate, incommensurate, high or low density per unit area). Safran took this as justification for constructing a model phase diagram in which in-plane long-range order and possible commensurate lock-in between guest and host layers were neglected.[14] One might similarly expect to find ordered 2D channel superlattices in doped polymers, independent of (or only weakly dependent on) the 1D filling fraction. This prediction is supported by the x-ray literature on alkali-metal-doped $(CH)_x$, where one finds examples of commensurate,[7,8] incommensurate,[11,12] and sometimes disordered[12,15] alkali-metal channels, all existing within the same 2D superlattice.

It thus seems that the inter- and intrachannel interactions can be roughly separated into "hard" and "soft" degrees of freedom, respectively. Indeed the most dramatic effects in $V_{OC}(y)$ for $[(CH)K_y]_x$ are associated with transitions in the *(a,b)* plane,[12] while weaker singularities in $V_{OC}(y)$ are suggestive of more subtle intrachannel transitions.[6] One can argue that the interchannel long-range order embodied in the 2D superlattice is ultimately derived from the local symmetry of the chain-plus-channel motif, which in turn should be only weakly dependent on channel filling fraction. Thus our focus in this paper is on the structures normal to the chain axis as revealed by equatorial (HK0) Bragg reflections; we consider reflections with finite L only to the extent necessary for a correct identification of in-plane reflections. The evolution of intrachannel order with y is an important issue that has yet to be experimentally addressed in detail.

Mean-field calculations for doped polymers and layer intercalates yield qualitatively similar phase diagrams,[13,14] indicating that entropic effects are comparable in the two systems; in both dimensionalities the guest sublattice reduces to isotropic random impurities at high T independent of y. On the other hand, volume considerations are quite different in the two cases. Graphite expands along the c axis to accommodate the intercalated layers, but this has no influence on the superlattice structure *per se* and only a quantitative effect on the predicted phase boundaries.[16] Polymer doping is fundamentally different, in that cooperative chain rotations and translations are required to open up channels for the intercalate to occupy. The resulting structure, *including the 2D superlattice symmetry*, depends on the relative sizes of the intercalate and the projection of the polymer chains.

The *(a,b)* plane symmetries of most pristine crystalline polymers are nearly triangular at 300 K. Small alkali metals [Li or Na in $(CH)_x$, Na or K in PPV] induce chain rotations in $(CH)_x$ and in PPV which leave this underlying symmetry unchanged, each channel being surrounded by three chains in the fully doped phases.[11,15,17,18] Larger alkali metals force both dilation and rotation leading to new symmetries, typically square *(a,b)* lattices in which each channel is surrounded by four chains.[1,7–9,12] (In the fully doped stage-1 phase, each chain is shared by two channels so the overall concentration is two chains/channel). Rb-doped PPV exhibits a complicated and highly disordered *(a,b)* plane structure, a borderline case between K-PPV and Cs-PPV.[19]

Guest-host and guest-guest interaction energies in graphite intercalation compounds are reasonably well understood. For example, long-range interlayer guest-guest Coulomb repulsion is the main driving force for staged layer superlattices. Since the electron charge transferred to the graphite layers from alkali-metal intercalates is delocalized in a graphitelike 2D π^* conduction band, the problem is reduced to a one-dimensional direct ionic interaction, albeit with complicated screening by the intervening graphite layers in high-stage structures. Analogous energies certainly play a role in stabilizing the local structures of the projected chain-plus-channel motifs in doped polymers, but the thermally averaged sizes and shapes of the chain and channel projections are likely to add an important new steric contribution to the motif symmetries.[20]

The top row of schematic *(a,b)* plane structures in Fig. 1 shows the undoped phase and three possible stage-2 superlattice structures (four chains surrounding each channel). The herringbone pattern in Fig. 1(a) is typical of

many crystalline polymers, including $(CH)_x$, polyethylene $[(CH_2)_x]$, and PPV $[(C_6H_8)_x]$. The 3D cell is monoclinic and its 2D projection is described by the *P2gg* space group. The small filled circles represent one arrangement of potential channel centers to be occupied in a stage-2 structure.

Figure 1(b) shows the highly symmetric stage-2 model proposed by Billaud *et al.* on the basis of x-ray diffraction from a sample of approximate composition $[(CH)K_{0.06}]_x$ (Ref. 21) (2D space group *P4mm*). This is derived from the pristine structure, Fig. 1(a), by expanding *a*, contracting *b*, and rotating every chain by $\pm 45°$; the filled channels lie on the corners of a primitive square lattice. This model results in conspicuously empty channels, which are then postulated to become occupied upon transformation from stage 2 to stage 1. Figure 1(c) shows an alternative proposal by Murthy *et al.*[7] for the stage-2 structure. The *(a,b)* cell is now centered rectangular (space group *Cmm*), and is derived from Fig. 1(a) by minor expansions of *a* and *b*. Note that half the chains must rotate by 90° to obtain Fig. 1(c) from Fig. 1(a). The void space is more diffuse than in Fig. 1(b); conspicuously empty channels are no longer present. Figure 1(d) shows the model (square lattice, space group *P4*) that best represents our data for the stage-2 structure, as described below in Sec. III. The cell has the same dimensions as the cell in Fig. 1(b) but only minor chain rotations relative to Fig. 1(a) are required. The distinguishing feature of our model is a motif that lacks the mirror planes of the other two. As a consequence, the hydrogens on the ends of adjacent chains are no longer at minimum separation, contrary to a prediction based on simple bonding arguments.[22] Within experimental error, the area per channel is the same in all three models, so there is no strong preference for one over the others based on free volume. On the other hand, the "unoccupied area" in Fig. 1(d) is highly delocalized whereas in Fig. 1(b) it is concentrated in the empty channels; Fig. 1(c) implies strips of unoccupied area between rows of occupied channels.

The bottom row in Fig. 1 shows similar models for stage-1 phases. Figure 1(e), the *P4mm* high-symmetry analog of Fig. 1(b) obtained by filling the remaining channels, has been the basis of numerous analyses of x-ray data for $(CH)_x$ doped to saturation with K, Rb, or Cs.[1,7,9,12,21] A general distortion from this high-symmetry motif can be represented by some combination of the "normal modes" shown in Figs. 1(f)–1(h). In Fig. 1(f) the chains are rotated about their centers with no change in space group. This distortion dominates in Cs-PPV (Sec. V). A similar motif on an oblique *(a,b)* lattice was proposed for K-$(CH)_x$ based on neutron-diffraction data,[10] whereas all the x-ray analyses agree on a tetrago-

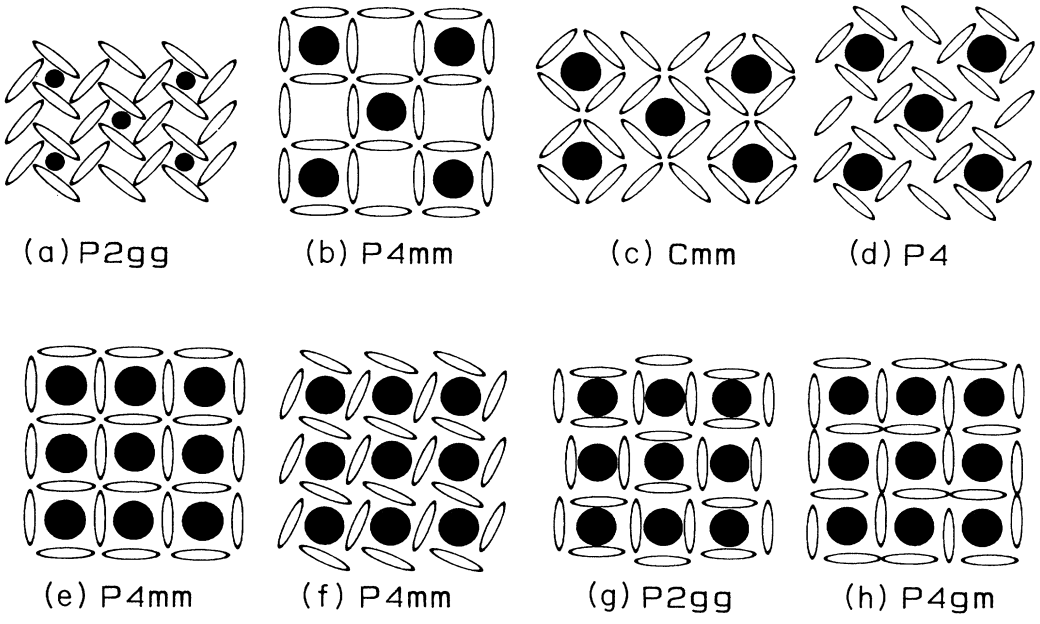

FIG. 1. Schematic *(a,b)* plane projections of pristine and doped polymer structures, and the associated 2D space groups. Filled circles represent intercalate channels and open ellipses represent polymer chains. (a) Undoped phase (*P2gg*), indicating one possible arrangement of channel centers which can develop into a stage-2 superlattice (small filled circles). (b) Highly symmetric *P4mm* structure (Ref. 21) for stage-2 K-$(CH)_x$. Only the channels indicated by filled circles are occupied. (c) Centered-rectangular model, space group *Cmm* (Ref. 7) for stage-2 K-$(CH)_x$. (d) Our proposed *P4* structure for stage-2 K-$(CH)_x$. (e) Highly symmetric *P4mm* structure for stage 1, derived from (b) by filling the unoccupied center channels. (f) Stage 1 with rotated chains, also *P4mm*. (g) Stage 1 with chains translated normal to their long axes, space group *P2gg*. (h) Stage 1 with chains translated parallel to their axes, space group *P4gm*.

nal 3D cell (Sec. IV). Figure 1(g) represents a translational distortion in which chains move towards some channels and away from others, in a manner that might be described as an asymmetric breathing mode. This distortion reduces the symmetry from *P4mm* to *P2gg*, with the consequence that some previously forbidden reflections become allowed. This distortion plays a role in the most recent analysis of K-$(CH)_x$ x-ray data by Billaud *et al.*[23] and Saldi *et al.*[24] Figure 1(h) is another translational distortion in which the direction of chain motion is normal to an axis connecting two channels (asymmetric shear mode, space group *P4gm*). We argue in Sec. IV that this model gives the best fit to x-ray data for saturation-doped K-$(CH)_x$. Since the *P4gm* space group has the same selection rules as *P2gg*, a careful intensity analysis is required to distinguish between breathing and shear translations.

All four stage-1 models are square lattices in the *(a,b)* plane, with the same area per channel; once again volume considerations offer no help in choosing among them. The remarkable fact is that independent analyses of three different doped phases (Secs. III, IV, and V to follow), lead to three different *structures*, Figs. 1(d), 1(f) and 1(h), constructed of *motifs* which are locally quite similar. In all three cases the chain projections either translate or rotate in such a manner that one chain end approaches the channel center while the other end moves away from it. In the high-symmetry structures, Figs. 1(b), 1(c) and 1(e), both ends of all chains are equidistant from the nearest channel centers. This similarity in *local* configurations suggests a common origin for the broken-symmetry motifs.

III. STAGE-2 K-$(CH)_x$

Figure 2 shows an x-ray powder-diffraction profile obtained at $y = 0.06$ during electrochemical dedoping of an unoriented Shirakawa-type $(CH)_x$ sample from the saturation value of $y = 0.17$. (Details of the diffractometer and electrochemical cell are presented in Ref. 12.) The Bragg peaks can all be indexed as (HK0) reflections of a square lattice with $a = 8.14$ Å. There is also a large broad peak centered near 1.4 $Å^{-1}$ due to diffuse scattering from the glass cell and from electrolyte-solvent condensed on the sample surface. The absence of (00L) and (HKL) reflections is significant. Calculations show that the (HKL) intensities are dominated by the metal form factor, while the (00L) reflections are too weak to be observed in our experiment.[9] Therefore, regardless of whether the metal and host sublattices are commensurate or incommensurate along the *c* axis, long-range metal order along *c* would be revealed by (HKL) reflections. The absence of such reflections in our data could be indicative of a large intrachannel Debye-Waller factor,[9] a short intrachannel correlation length, or lack of correlation between different channels, leading to broad and weak (HKL) reflections in a powder profile. Experiments by Saldi *et al.*[24] on oriented samples show that these reflections are sharp along Q_L but severely streaked along Q_H and Q_K, supporting the third hypothesis: for stage 2, the K ions

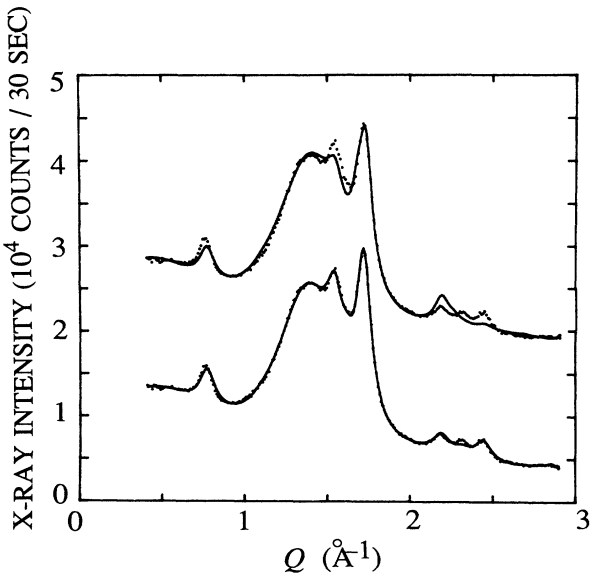

FIG. 2. X-ray diffraction from *in situ* electrochemically doped, unoriented stage-2 K-$(CH)_x$. Upper curve shows best fit to the Fig. 1(b) model, with unoccupied center channels. Lower curve shows best fit with the symmetry-breaking distortion of Fig. 1(d).

exhibit long-range intrachannel order but little or no interchannel order.

The *P4mm* and *P4* models, Figs. 1(b) and 1(d), were tested by least-squares fitting entire profiles to calculated diffraction patterns. For a given model, the fitting variables were the lattice constant *a*, a constant width for the Lorentzian-broadened Bragg peaks, the relative occupancies of filled and empty channels, and projected chain center positions and setting angles. For *P4mm*, the projected chain centers were fixed at (0.25, 0.25) with a 45° setting angle. For *P4* the optimal setting angle was determined by initial fits to be close to 0° and was subsequently fixed at that value, while the chain centers were optimized within the least-squares procedure. Model-independent variables were a quadratic background function, a broad Lorentzian representing glass and solvent scattering, the overall amplitude, and anisotropic C and K thermal factors. We also included a variable amount of undoped material, the parameters of which were fixed by a profile fit to a monoclinic structure at nominal $y=0$. For both the *P4mm* and *P4* models, we found $a = 8.145$ Å and rms C and K thermal displacements less than 0.1 Å; the latter were fixed at zero in the final fits. In both cases the best initial fits gave center channel occupancies very close to zero, and the occupancy was fixed at zero in subsequent fits. Both models do an adequate job of indexing the observed (HK0) peak positions; differences lie in the predictions of peak intensities.

The best fit based on the *P4mm* model, Fig. 1(b), is shown as the upper curve in Fig. 2. The lower curve shows the best fit with the *P4* model, Fig. 1(d). The improvement is obtained by rotating the chains 45° about their centers and translating their centers of mass from

(0.25, 0.25) to (0.18, 0.31), which greatly reduces the area of the empty channels. This gives much better agreement with all the observed (HK0) intensities, especially with the weak (220), (300), and (310) peaks in the range 2.1-2.5 $Å^{-1}$. In Fig. 3 we compare background-subtracted data in this range with (HK0) profiles calculated from all three models assuming $y = 0.07$. Experimentally (filled squares), peaks at $Q = 2.18$ and 2.44 $Å^{-1}$ have roughly equal intensities, in accord with the *P*4 prediction (top curve). With the *P*4*mm* assumption (bottom curve), the former is four times as intense as the latter, while the *Cmm* assumption (middle curve) predicts an even larger peak at 2.18 $Å^{-1}$ and no peak at 2.44 $Å^{-1}$. The *Cmm* assumption is also incompatible with the lowest-order reflection at 0.76 $Å^{-1}$ (Fig. 2); this would be an unresolved doublet with roughly twice the width of other (isolated) (HK0) reflections.

Experimentally, the strongest reflection occurs at 1.7 $Å^{-1}$, close to the position of the (020)-(110) doublet in pristine *trans*-$(CH)_x$. The *P*4*mm* and *Cmm* models both contain reflections at this Q, but with intensities only 20–25 % of the strongest reflection. This led the authors of Ref. 7 to invoke the coexistence of stage 2 with a substantial fraction of undoped material. Thus, optimizing the fit to the *P*4*mm* model required that more than 90% of the intensity of this peak be assigned to residual *trans*-$(CH)_x$. The *P*4 model can account for all of this intensity as the (210) reflection, although the best overall fit still requires attributing 30% of the 1.7 $Å^{-1}$ intensity to residual *trans*-$(CH)_x$. Indeed, every nominally stage 2 x-ray pattern that we have measured is best described by a mixture of stage 2 with either *trans*-$(CH)_x$ or stage 1. It is unclear at this stage whether this implies that (a) stage-2 is truly never present as a pure phase, (b) our steps in y were too large, (c) our relatively large $(CH)_x$ electrode was never in uniform equilibrium (despite the high porosity of Shirakawa material), or (d) the optimization of the fits by the inclusion of other phases simply represents the fact that *any* least-squares fit is improved by the addition of new free parameters.

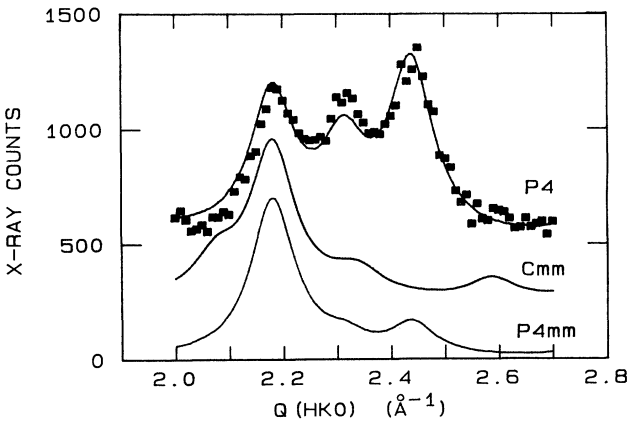

FIG. 3. Blow-up of data from Fig. 2 with background subtracted (solid dots), compared with three models: the highly symmetric *P*4*mm* model of Fig. 1(b) (bottom); the centered-rectangular *Cmm* model of Fig. 1(c) (middle); and the low-symmetry *P*4 model of Fig. 1(d) (top). All profiles have been scaled to the peak at 2.18 $Å^{-1}$.

The differences among the three predicted profiles are sufficiently large that relaxing the assumption of a Q-independent width has no effect on our conclusion that *P*4 is the correct symmetry. Furthermore, it is unlikely that the *P*4 fit would be materially improved by allowing a Q-dependent width. This seems to be a general feature of (HK0) reflections in alkali-metal-doped $(CH)_x$,[9,12] suggesting that paracrystalline interchain or interchannel disorder[25] is relatively unimportant.

Figure 1(d), which is a schematic diagram of our stage-2 *P*4 model, represents the charge density from the $(CH)_x$ chains *projected* onto the *(a,b)* plane as featureless ellipses. In reality, the chains have a zig-zag structure along the *c* axis, so that a *cut* in any particular plane should in fact represent the ellipses as arrows, with the sense of the arrow distinguishing a "zig" from a "zag." This directional aspect becomes important when neighboring chains touch, at which point head-to-tail interactions are clearly different from head-to-head interactions. We can thus expect that the directions of the arrows in any given plane will be ordered, possibly doubling the *(a,b)* plane periodicity. This new order, however, cannot result in any modification of the (HK0) intensities, and will most likely only modify the already very weak $(CH)_x$ contribution to the (HKL) reflections.

IV. STAGE-1 K-$(CH)_x$

To examine the structure of stage-1 K-$(CH)_x$, we studied both the unoriented sample discussed above, doped electrochemically to saturation, and also an oriented vapor-doped sample. In both cases the diffraction profiles were subjected to least-squares fits with various assumed models. Model-independent parameters were quite similar to those from stage-2, although the cell lattice parameter increased to $a = 8.41$ Å.

Figure 4 shows an (HK0) profile from an oriented K-$(CH)_x$ sample (*c*-axis mosaic FWHM 40°), vapor-doped to saturation and transferred under argon into a beryllium cell that was evacuated and gettered with freshly cut sodium. X-ray measurements were performed as in Ref. 12 except that Mo $K\alpha$ radiation and a four-circle goniometer were employed. This profile is consistent with our *in situ* powder data in the range $0.09 < y < 0.16$.[12] The upper solid curve compares the data with the best fit to the high-symmetry *P*4*mm* model, Fig. 1(e). This model correctly predicts the positions of most of the observed peaks, but with substantial errors in relative intensities. More significantly, all of the observed intensity at 1.68 $Å^{-1}$ would have to be attributed to the (020)-(110) doublet of undoped $(CH)_x$ since there are no model (HK0)'s in this Q range. In Sec. III we discussed the possible persistence of undoped $(CH)_x$ at y values as high as 0.06; it seems unlikely that any significant amount would remain in the case of vapor-doping (which is less likely to be nonuniform) to saturation. We therefore argue that all

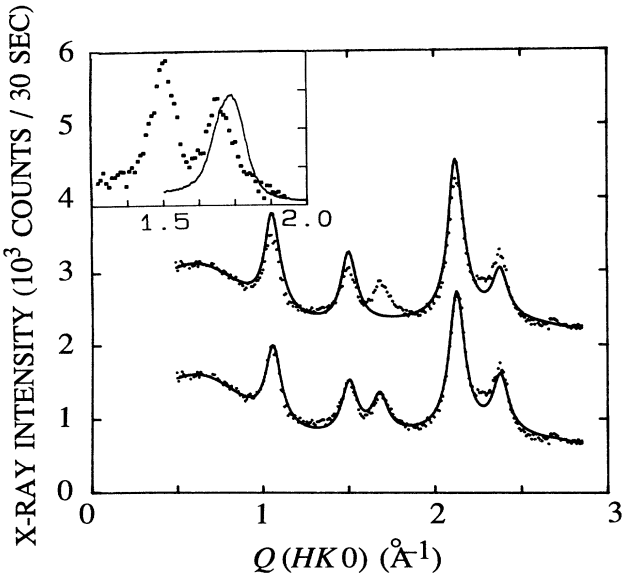

FIG. 4. X-ray diffraction from vapor-doped, oriented stage-1 K-$(CH)_x$. Upper curve shows best fit with the *P4mm* model for stage-1 [Fig. 1(e)]. Lower curve shows best fit with the *P4gm* symmetry-breaking distortion of Fig. 1(h). Inset: solid points are a blow-up of the 1.25−2.00 Å^{-1} region of the same data. Solid curve traces data for pristine *trans*-$(CH)_x$. Note the difference in peak positions.

the intensity at 1.68 Å^{-1} in Fig. 4 must be attributed to the (210) reflection of the low-symmetry *P4gm* structure, Fig. 1(h). The lower curve in Fig. 4 compares the data with the best fit to this model, which accounts quite well for the positions and intensities of all the observed (HK0) reflections.

We studied the 1.68-Å^{-1} peak in more detail since this region is most sensitive to differences among alternative model structures. Azimuthal scans at fixed $Q = 1.68$ Å^{-1} show unambiguously the existence of (101) and (10$\bar{1}$) reflections at roughly the same Q as the (210), from which we deduce $c = 4.2$ Å. This identification is consistent with the film data of Saldi and co-workers.[8,24] The (101) and (10$\bar{1}$) are highly streaked along Q_H and Q_K due to limited interchannel correlations. Mathis *et al.* identified this scattering with an (00L) reflection in an orthorhombic cell with c as the unique axis.[26] The strongest argument against this identification is that the predicted (00L) intensities in essentially any structural model are far too weak to account for the observations. We also find that the component of this peak in the (HK0) plane has a measurably different radial position from that expected for undoped *trans*-$(CH)_x$, as shown in the inset for Fig. 4. The undoped peak is also broader, revealing its doublet nature. We conclude that both our saturation vapor-doped sample and our *in situ* sample with $0.09 < y < 0.16$ are best described as *single-phase* stage 1, with no measurable remnant of undoped material, and that the *P4gm* model best describes the observed profiles.

The optimized fit allowing for broken symmetry (lower curve in Fig. 4) was obtained by letting the three displacements [Figs. 1(f)–1(h)] vary independently. We find that a parallel displacement of 0.36±0.08 Å along the chain major axes [Fig. 1(h)] is the predominant effect, and the fit shown utilized only this displacement. A displacement of this magnitude is sufficient to bring the projections of the H's into contact; this can be avoided or reduced by translating alternate chains along c. The fit is not improved by allowing an additional rotation distortion as in Fig. 1(f), although for $(CH)_x$-based phases (unlike PPV, as discussed below), the x-ray structure factor is not very sensitive to rotations. A similar *motif* distortion exists in the orthorhombic cell proposed by Aime *et al.*,[10] for which either a or b is the unique axis. While our data would not be inconsistent with a setting angle rotation of 15° relative to the *P4gm* structure (as required by the Aime model), we see no evidence for the inferred orthorhombic splitting of (HK0) reflections. It is difficult to distinguish between parallel (*P4gm*) and normal (*P2gg*) displacements since the selection rules on (HK0) reflections are identical. Numerically, we find that the pure parallel displacement gives a better overall fit to the observed intensities than a pure normal displacement of similar magnitude. The former is also more appealing on physical grounds; it results in a *motif* which closely resembles that of stage 2 [Fig. 1(d)], and also avoids the necessity of moving two of the four neighboring chain projections 0.36 Å closer to the channel center (which would probably lead to overlapping C and K densities).

The fact remains that the latest analysis by Saldi *et al.*[24] advocates this distortion, in combination with an asymmetric rotation. We were unable to test this combined distortion in detail since these authors did not give the atomic positions. We can also rule out unequal filling of corner and center channels,[23] since this would introduce nonzero (100) intensity that is not observed. Note that the center-of-mass positions of the chains in our low-symmetry stage-1 and stage-2 structures are very similar. The system apparently evolves from stage 2 to stage 1 by an almost pure rotation of the chains, together with a ~3% lattice expansion, to form an occupied center channel.

The c-axis periodicity of 4.2 Å inferred from the (101) peak at 1.7 Å^{-1} suggests that the K channels are incommensurate with the (CH) backbone, as is also found for heavily Cs-doped $(CH)_x$ (Ref. 9) and PPV (Ref. 19). It appears likely that the *(a,b)* plane symmetry breaking will affect the c-axis correlations; in-plane steric forces may impose specific staggering of the $(CH)_x$ chains, which in turn can influence the equilibrium configuration of intercalates within a channel, leading variously to commensurate, incommensurate, or disordered phases. These questions can be addressed by *in situ* experiments on highly-oriented samples, focusing on (00L) and (HKL) reflection families.

V. STAGE-1 Cs-PPV

Samples were prepared by vapor doping of highly oriented films 10 μm thick,[18] mounted in thin-wall glass

capillaries. X-ray measurements were performed using Cu $K\alpha$ radiation. Doping was performed with the sample on the goniometer in order to control the Cs concentration necessary for achieving a stage-1 channel superlattice. Unlike the stage 1 K-$(CH)_x$ samples that could be obtained as pure phases, PPV doped with enough Cs to establish stage 1 also exhibits small residues of undoped PPV, and/or evidence of further evolution to a more dense structure.

Figure 5 shows a typical equatorial (HK0) scattering profile after doping to stage 1. All of the peaks can be nominally indexed by a 2D nonprimitive square lattice with $a = 9.63$ Å, a value that is larger than the 9.1 Å found in stage-1 Cs-doped $(CH)_x$.[9] Since the PPV chain projection represents a larger rotor than that of $(CH)_x$, only the Cs ion is sufficiently large to stabilize a fourfold channel structure in PPV.[19] Hence, the crossover from a threefold to a fourfold channel structure with increasing relative alkali-metal size is a general feature of polymer intercalation. A full 3D analysis is consistent with a highly-faulted staggered packing of the Cs ions.[19] A weak scattering feature at 1.48 $Å^{-1}$ is observed in the raw data. This is a signature of a small amount of undoped PPV. Since the scattering profile of undoped PPV is substantially different from that attributed to stage-1 Cs-PPV, the undoped "impurity phase" can easily be incorporated into the background profile, along with scattering by air, the sample holder, and weak powder peaks from CsCl residues.

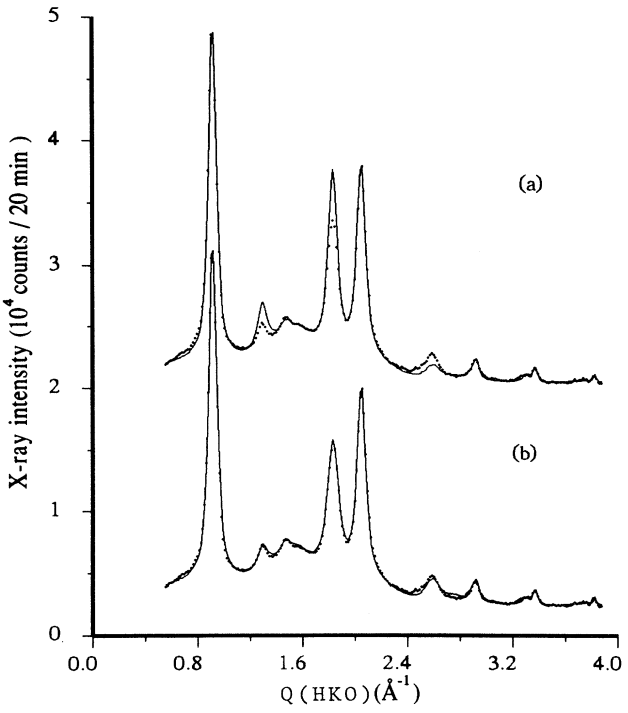

FIG. 5. Equatorial (HK0) x-ray-diffraction profile from vapor-doped, oriented, stage-1 Cs-PPV. Experimental diffraction profiles are shown with black dots, models with solid lines. The top curve shows the best fit to the standard model, Fig. 1(e), while the bottom curve employed the chain-axis rotation of Fig. 1(f).

In the previous section we showed that stage-1 K-$(CH)_x$ is well represented by a broken-symmetry model consisting solely of chain translations relative to the hypothetical high-symmetry structure of Fig. 1(e). The signature for that transformation was a reduction in space-group symmetry from *P4mm* to *P4gm*, which gave rise to new Bragg reflections. In contrast, we find no evidence for symmetry-forbidden peaks (with respect to *P4mm*) for stage-1 Cs-(PPV). We find instead a *motif* with lower symmetry but no change in 2D space group. This modification of the high-symmetry *motif* involves only chain rotations, Fig. 1(f), as revealed by systematic differences in the relative intensities of some Bragg reflections as compared to the *P4mm* model, Fig. 1(e).

The *P4mm* model without chain rotations, the top curve in Fig. 5, does not yield an acceptable fit to the data. There are significant differences between measured and predicted integrated intensities for the (200) at 1.30 $Å^{-1}$, the (220) at 1.84 $Å^{-1}$, and the (400) at 2.61 $Å^{-1}$. The phenyl rings within the PPV backbone dramatically increase the sensitivity of diffraction intensities to rotations about the chain axis as compared to $(CH)_x$. A significant improvement in the fit is achieved with chain rotations of $23\pm3°$, as shown in the bottom curve of Fig. 5. It is significant that this single distortion removes the discrepancies in all three reflections mentioned above, without appreciably affecting the good agreement that existed for all other reflections before introducing the distortion.

The major effect of this rotation is to increase the projected average H-H interchain distance and to reduce the minimum spacing between alkali dopants and polymer chains as compared to Fig. 1(e). The absence of measurable translations may arise from different steric effects in Cs-PPV and K-$(CH)_x$. The projected relative areas of Cs and PPV are more closely matched to those of Rb and $(CH)_x$. Furthermore, guest-host interactions are expected to differ significantly, since PPV and $(CH)_x$ have very different local geometries in which to distribute excess charge. Even the intrachain electronic excitations should be substantially different in the two polymers since only $(CH)_x$ exhibits a degenerate ground state in the undoped phase.

The (HK0) reflections are sensitive only to the mass density projected onto the *(a,b)* plane, and their intensities are dominated by the atoms in the rings. Thus we cannot distinguish between uniform rigid chain rotations and systematic phenylene ring rotations of $\pm23°$ about the backbone axis. A dominant contribution from the latter possibility is unlikely because the doping-induced charge transfer process generates appreciable double-bond character across the vinyl-phenyl C-C linkage that should inhibit these large-scale angular displacements. Moreover, ring rotations relative to fixed backbone planes would bring the phenyl-ring hydrogens on neighboring chains into close proximity such that repulsive steric effects would become important.

VI. SUMMARY AND CONCLUDING REMARKS

We have shown for 3 distinct cases that the chain-plus-channel motifs in alkali-metal-doped polymers adopt a symmetry that is lower than would be predicted on the basis of simple bonding and packing considerations.[22] For example, the projected H-H interchain distance is not minimized equally for all pairs, the axis of one chain in the *(a,b)* plane is not a perpendicular bisector of its neighbors, etc. Work in progress on Li-doped $(CH)_x$ indicates that broken symmetries also exist with "small" dopants, for which the channels are defined by three rather than four neighboring chain projections.[27] This suggests that the effect originates in some general aspect of the *(a,b)* plane interaction between host chains and metal-filled channels that has not been considered heretofore. Factors governing the equilibrium structure in the *(a,b)* plane include chain-channel, chain-chain, and channel-channel interactions, both steric and Coulomb, more complicated quantum effects, and, at finite temperature, the entropy. We close by discussing three candidates for the symmetry-breaking interaction.

One of the key assumptions justifying high-symmetry motifs is that the electron density associated with carbon sigma orbitals resides exactly midway between C atoms on a given chain;[22] thus in projection there is no electric dipole moment. This ignores the possibility of π-σ hybridization induced by the nearby metal ion, and/or metal-carbon hybridization, both of which are non-negligible in graphite intercalation compounds.[28] This possibility could be addressed by a self-consistent version of the calculation by Kertesz *et al.*,[29] allowing for relaxation of the chain centers and orientations within a lattice of ionized dopant channels.

A finite electric dipole moment normal to the chain axis is also a direct consequence of the charge oscillations associated with soliton or polaron defects.[30] The oscillation period is one site, the decay length away from an isolated defect is of order 7 sites, and the maximum amplitude of the charge alternation between neighboring sites is of order 0.3 electron units (near the center of the defect). Chains surrounding a channel would therefore be expected to rotate such that the positive ends of the dipoles get closer to the channel center, which under the right circumstances could reproduce the low-symmetry motifs in Fig. 1. For solitons in doped $(CH)_x$, it seems unlikely that this mechanism would be effective on the relevant intrachain length scale (of order 100 Å) since at high density the alternating dipoles associated with closely spaced soliton-antisoliton pairs would cancel in projection resulting in no net moment. This restriction need not apply to polarons,[30] thus the mechanism may be operative in doped PPV. In either case, attribution of the symmetry breaking to this mechanism would lend support to the soliton and/or polaron lattice models of the metallic state.[31]

The importance of both rotational and translational degrees of freedom is underscored by results obtained from the mean-field anisotropic rigid rotor model of Choi *et al.*[20] This model emphasizes steric effects by representing the projected channel and chain mass densities as discs and multipole expansions, respectively, including higher-order terms to describe interchain and chain-channel interactions. The model correctly predicts the existence of a 2D incommensurate channel structure in Na-doped $(CH)_x$,[15] a situation in which the rotational degrees of freedom dominate since both the doped and undoped phases are essentially triangular lattices with nearly the same lattice parameter. Conversely, the model fails to account for the anisotropic thermal expansion of *trans*-$(CH)_x$ in the *(a,b)* plane[32] since the translational degrees of freedom were neglected. It seems possible that an appropriate combination of high-order terms in the mass density expansion, allowing for coupled rotations and translations, could reproduce the observed motif symmetries. Of greater importance at present is the prospect of classifying the hierarchy of observed channel structures (broken symmetry, incommensurate, and disordered) according to the specific channel and chain mass densities encountered in the whole range of doped conjugated polymers.

The theory of doped conjugated polymers is now starting to advance beyond the single-chain approximation.[33] Structure models based on diffraction analyses are being used as the basis for calculations of electron structure, optical and magnetic properties, etc. In principle, the interchain interactions predicted from the "standard" 3D structure models will be strongly modified by the broken symmetries reported here. Overlap integrals between π orbitals on near-neighbor chains, and those between dopant and host, may be orders of magnitude different when the *(a,b)* plane rotations and translations are taken into account. This in turn could have profound consequences on the various debates concerning the dimensionality of electron transport, magnetism, and other macroscopic properties. Furthermore, it is not unrealistic to expect before long the appearance of the first prediction of an equilibrium doped 3D structure based on a total energy minimization. One hopes that the results represented here will help provide a rational basis for progress along these lines.

ACKNOWLEDGMENTS

We acknowledge helpful conversations with R. H. Baughman, E. J. Mele, A. B. Harris, and B. H. Toby. We thank S. H. J. Idziak for his technical assistance. This work was supported by NSF Materials Research Laboratory Grant No. DMR88-19885 (P.A.H., J.M), by U.S. Department of Energy Grant No. DEFG02-87ER45254 (J.E.F, D.D), by the University of Wisconsin (D.C.), by NSF Division of Materials Research Grant No. DMR-8917530 (M.J.W.), and by the AFOSR (F.E.K.). The Penn-Montpellier collaboration is supported by NATO Grant No. 0866/87.

*Also at Department of Physics, University of Pennsylvania, Philadelphia, PA.
†Also at Department of Materials Science and Engineering, University of Pennsylvania, Philadelphia, PA.
‡Current address: Laboratoire de Chimie des Solides, Universite Blaise Pascal, 63177 Aubiere CEDEX, France.
§Current address: Department of Materials Science and Engineering, University of Pennsylvania, Philadelphia, PA.

[1]R. H. Baughman, N. S. Murthy, and G. G. Miller, J. Chem. Phys. **79**, 515 (1983).
[2]L. W. Shacklette, N. S. Murthy, and R. H. Baughman, Mol. Cryst. Liq. Cryst. **121**, 201 (1985).
[3]A. Metrot and J. E. Fischer, Synth. Met. **3**, 201 (1981).
[4]C. Fite and P. Bernier, Phys. Rev. B **36**, 4574 (1987); N. Coustel, C. Fite, and P. Bernier, Mater. Sci. Forum **42**, 143 (1989).
[5]L. W. Shacklette and J. E. Toth, Phys. Rev. B **32**, 5892 (1985).
[6]N. Coustel, P. Bernier, and J. E. Fischer, Phys. Rev. B **43**, 3147 (1991).
[7]N. S. Murthy, L. W. Shacklette, and R. H. Baughman, Phys. Rev. B **41**, 3708 (1990).
[8]F. Saldi, J. Ghanbaja, D. Begin, M. Lelaurain, and D. Billaud, C. R. Acad. Sci. **309**, 671 (1989).
[9]J. Ma, D. Djurado, J. E. Fischer, N. Coustel, and P. Bernier, Phys. Rev. B **41**, 2971 (1990).
[10]J. P. Aime, M. Bertault, P. Delannoy, R. L. Elsenbaumer, G. G. Miller, and M. Schott, J. Phys. (Paris) Lett. **46**, L379 (1985).
[11]O. Leitner, H. Kahlert, G. Leising, J. Fink, and H. Fritzsche, Synth. Met. **28**, D225 (1989).
[12]D. Djurado, J. E. Fischer, P. A. Heiney, J. Ma, N. Coustel, and P. Bernier, Synth. Met. **34**, 683 (1990).
[13]J. Ma, H.-Y. Choi, E. J. Mele, and J. E. Fischer, Synth. Met. **27**, A75 (1988).
[14]S. A. Safran, in *Chemical Physics of Intercalation* edited by A. P. Legrand and S. Flandrois (Plenum, New York, 1987), p. 47.
[15]M. Winokur, Y. B Moon, A. J. Heeger, J. Barker, D. C. Bott, and H. Shirakawa, Phys. Rev. Lett. **58**, 2329 (1987).
[16]S. E. Millman and G. Kirczenow, Phys. Rev. B **28**, 3482 (1983).
[17]N. S. Murthy, L. W. Shacklette, and R. H. Baughman, Phys. Rev. B **40**, 12 550 (1990).
[18]D. Chen, M. J. Winokur, M. A. Masse, and F. E. Karasz, Phys. Rev. B **41**, 6759 (1990).
[19]D. Chen, M. J. Winokur, and F. A. Karasz, Synth. Met. **41**, 341 (1991).
[20]H. Y. Choi and E. J. Mele, Phys. Rev. B **40**, 3439 (1989); H. Y. Choi, A. B. Harris, and E. J. Mele, *ibid.* **40**, 3766 (1989).
[21]D. Billaud, J. Ghanbajha, and C. Goulon, Synth. Met. **17**, 497 (1987).
[22]R. H. Baughman, L. W. Shacklette, N. S. Murthy, G. G. Miller, and R. L. Elsenbaumer, Mol. Cryst. Liq. Cryst. **118**, 253 (1985).
[23]D. Billaud, F. Saldi, J. Ghanbaja, D. Begin, and M. Lelaurain, Synth. Met. **35**, 113 (1990).
[24]F. Saldi, M. Lelaurain, and D. Billaud, Solid State Commun. **76**, 595 (1990).
[25]J.-P. Pouget, in *Electronic Properties of Polymers and Related Compounds*, Springer Series in Solid State Sciences, Vol. **63**, (Springer-Verlag, Berlin, 1985), p. 26.
[26]C. Mathis, R. Weizenhofer, G. Leiser, V. Enkelmann, and G. Wegner, Makromol. Chem. **189**, 2617 (1988).
[27]C. Mathis, V. B. Cajipe, B. M. Powell, J. Ma, Q. Zhu, and J. E. Fischer (unpublished).
[28]C. T. Chan, W. A. Kamitakahara, K. M. Ho, and P. C. Eklund, Phys. Rev. Lett. **58**, 1528 (1987).
[29]M. Kertesz, F. Vondeviszt, and S. Pekker, Chem. Phys. Lett. **90**, 430 (1982).
[30]D. S. Boudreaux, R. R. Chance, J. L. Bredas, and R. Silbey, Phys. Rev. B **28**, 6927 (1983).
[31]A. J. Heeger, S. Kivelson, J. R. Schrieffer, and W.-P. Su, Rev. Mod. Phys. **60**, 782 (1988).
[32]J. Ma, J. E. Fischer, C. Mathis, B. Francois, N. Coustel, P. Bernier, M. E. Josefowicz, E. M. Scherr, and A. G. MacDiarmid (unpublished).
[33]Proceedings of the International Conference on Synthetic Metals, Tubingen, Germany, 1990 [Synth. Met. (to be published)].